©2000, CIVIL-COMP Ltd., Edinburgh, Scotland
Z. Bittnar and B.H.V. Topping, (Editors),
Computational Concrete Structures Technology,
Civil-Comp Press, Edinburgh, 95-106.

THREE PARAMETERS DAMAGE MODEL FOR CONCRETE

A.R. Khan, A.H. Al-Gadhib and M.H. Baluch
Department of Civil Engineering
King Fahd University of Petroleum and Minerals
Dhahran, Saudi Arabia

Abstract

An effective compliance matrix $\widetilde{C}$ is proposed to model the behaviour of concrete based on phenomenological evidences and physical insight. Three parameters α, β and γ were introduced in the effective compliance matrix $\widetilde{C}$. α and β are introduced to model the different behaviour of concrete in tension and compression while the third parameter γ was introduced to account for volumetric change. The predictive capability of the proposed elasto-damage model for uniaxial and multiaxial stress path was investigated for uniaxial compression, biaxial compression and uniaxial tension. The predicted results correlate well with the available experimental data. The simulative capability of the model to capture the phenomenological behaviour of volumetric dilatation is reflected. Also, the ability of the model to predict multiaxial response of concrete is reflected through biaxial strength interaction envelope which compares very well with the experimental results.

1 Introduction

In recent years considerable research has been focused on modelling of mechanical behaviour of concrete. The mechanical behaviour of concrete is very complicated and the possible variations in material characteristics have not been modelled effectively under various theoretical frameworks such as non-linear elasticity [1–3], rate-independent plasticity [4–6], endochronic theory [7, 8] and plastic-fracturing theory [9, 10]. Typical trends in concrete behaviour include: stiffness degradation, strain softening, volumetric dilatation, different behaviour in tension and compression, and gain in strength under increasing confinement.

More recently, the theory of continuum damage mechanics (CDM) originally proposed by Kachanov [11] has been used extensively to model the progressive degradation of the mechanical properties of materials caused by microcracking. Concrete contains numerous microcracks, even before the application of the external loads. Under applied loading, the initiation of new microcracks and the growth of existing microcracks contribute to the observed nonlinear behaviour in concrete, ultimately causing the failure. The existence of microcracks and their propagation cause what is termed as "damage" to the concrete.

The effective stress-concept introduced by Kachanov [11] has been applied to concrete by Krajcinovic [12], Loland [13] and Mazars [14]. Scalar damage variable used by them was not sufficient to model the highly oriented cracking occurring in concrete under loading. Vectorial/tensorial damage variables were used to model this crack-induced anisotropy by Krajcinovic and Fonseka [15], Suaris and Shah [16], Kachanov [17], Cordebois and Sidoroff [18] and Ortiz [19]. The damage effect tensor $\underline{M}$ was proposed and used to cast the continuum damage theory for the general case of anisotropic damage in a consistent mathematical and mechanical framework by Chow and Wang [20, 21]. However, application of the work of Chow and Wang was limited to metals. The concept of bounding surface, first applied to metals by Dafalias and Popov [22], was applied to concrete by Fardis *et al.* [23], Suaris *et al.* [24], Voyiadjis and Abu-Lebdeh [25], Abu-Lebdeh and Voyiadjis [26], Yazdani and Schreyer [27] and Yazdani and Karnawat [28]. More recently, the concepts of damage effect tensor and bounding surface were used successfully to predict most of the essential features of normal and high strength concrete except volumetric dilatation by Khan *et al.* [29].

The present study is aimed towards developing a constitutive model for normal and high strength concrete able to capture all essential features of concrete including volumetric dilatation. This is achieved by proposing effective compliance matrix $\widetilde{C}$ based on phenomenological evidences and physical insight. Different behaviour of concrete in tension and compression is taken into account by introducing two parameters α and β, while the effect of volumetric dilatation is controlled by a third parameter γ. The constitutive relations and damage growth are derived using the approach presented by the authors in their previous work [29]. The proposed mode is simple, captures the constitutive behaviour of concrete and can be directly implemented into a general-purpose finite element code with relative ease.

2 Theoretical Preliminaries

2.1 Effective compliance matrix

Based on physical insight, the following compliance matrix $\underset{\sim}{\tilde{C}}$ is postulated

$$\tilde{C}_{11} = \frac{1}{E_o}\frac{(1-\beta\omega_1)^2}{(1-\alpha\omega_1)^2(1-\beta\omega_2)^2(1-\beta\omega_3)^2}$$

$$\tilde{C}_{22} = \frac{1}{E_o}\frac{(1-\beta\omega_2)^2}{(1-\alpha\omega_2)^2(1-\beta\omega_3)^2(1-\beta\omega_1)^2}$$

$$\tilde{C}_{33} = \frac{1}{E_o}\frac{(1-\beta\omega_3)^2}{(1-\alpha\omega_3)^2(1-\beta\omega_1)^2(1-\beta\omega_2)^2} \qquad (1)$$

$$\tilde{C}_{12} = -\frac{\nu 1}{E_o(1-\alpha\omega_1)(1-\alpha\omega_2)(1-\beta\omega_3)^2(1-\gamma\omega_1)(1-\gamma\omega_2)}$$

$$\tilde{C}_{13} = -\frac{\nu 1}{E_o(1-\alpha\omega_1)(1-\alpha\omega_3)(1-\beta\omega_2)^2(1-\gamma\omega_1)(1-\gamma\omega_3)}$$

$$\tilde{C}_{23} = -\frac{\nu 1}{E_o(1-\alpha\omega_2)(1-\alpha\omega_3)(1-\beta\omega_1)^2(1-\gamma\omega_2)(1-\gamma\omega_3)}$$

$$\tilde{C}_{22} = \tilde{C}_{12} \qquad \tilde{C}_{31} = \tilde{C}_{13} \qquad \tilde{C}_{32} = \tilde{C}_{23}$$

in which the thermodynamic constraint requirement

$$E_i\nu_{ji} = E_j\nu_{ij} \qquad (2)$$

has been insured.

2.2 Bounding surface

In order to construct a rational model accounting for damage growth, concepts are borrowed from incremental theory of plasticity in general and the bounding surface plasticity model in particular as introduced by Dafalias and Popov [22]. Plasticity bounding surface model as proposed by Dafalias, requires definition of multiple surfaces in stress space. However, the fundamental surfaces in the present work are best described in strain-energy release space, as proposed by Suaris *et al.* [24]

$$f = (R_i R_i)^{1/2} - R_c / b = 0 \qquad (3)$$

$$F = (\bar{R}_i \bar{R}_i)^{1/2} - R_c = 0 \qquad (4)$$

$$f_o = (R_i R_i)^{1/2} - R_o = 0 \qquad (5)$$

where, f is the loading function surface, F is the bounding surface, f_o is a limit fracture surface [24]. The loading function surface (f) is defined in terms of thermodynamic-force conjugates, R_i, where,

$$R_i = \rho\frac{\partial\Lambda}{\partial\omega_i}(\sigma_{ij}, \omega_i) \qquad (6)$$

where $\rho\Lambda$ is the strain energy density and $\bar{R}_i$ is an image point on $F = 0$ associated with a given point R_i on $f = 0$ defined by a mapping rule

$$\bar{R}_i = bR_i \qquad (7)$$

$$b = R_c/(R_i R_i)^{1/2} \qquad (8)$$

with the mapping parameter b ranging from an initial value of ∞ to a limiting value of 1 on growth of loading surface to coalesce with bounding surface. R_c, critical strain energy release rate, is a parameter of the model and is calibrated to the standard uniaxial compression test, and is suggested to be 1.29. R_o defines the initiation of microcracking which occurs at about 40% of the peak stress as indicated by experimental results, and it varies with the compressive strength of concrete as:

$$R_o = \sqrt{2}\beta(0.4 f_c')^2 / E_o \qquad (9)$$

Damage is hypothesized to accumulate at levels of strain energy release rate resulting in the loading surface (f) traversing the limit fracture surface (f_o) and rupture in the damage sense is said to occur when 'f' grows large enough to coalesce with the bounding surface F fixed in the R_i space.

It can be argued from the above discussion that R_c should also vary with the compressive strength of concrete, f_c', like R_o. At this point it seems appropriate to discuss the role of parameters α and β. It is true that R_c will vary with f_c', but with the introduction of α and β it does not matter that R_c is fixed or varying. α and β control the movement of the loading surface which describes the onset of damage or failure, i.e. higher values of α and β means faster movement of loading surface and hence lower peak stress, as it will reach the bounding surface much earlier than with lower values of α and β. This makes the model flexible enough to accommodate normal as well as high strengths of concrete.

2.3 Damage evolution

The damage growth is determined from the loading surface, f, as

$$d\omega_i = d\lambda\frac{\partial f}{\partial R_i} \qquad (10)$$

With $k = R_c / b$, equation of loading becomes

$$f(R_i, k) = (R_i R_i)^{1/2} - k(\bar{\omega}_p) = 0 \qquad (11)$$

where $\bar{\omega}_p$, the norm of accumulated damage is defined as,

$$d\bar{\omega}_p = C\,(d\omega_i\, d\omega_i)^{1/2} \quad (C \text{ is constant}) \tag{12}$$

Consistency condition $df = 0$

$$\frac{\partial f}{\partial R_i} dR_i + \frac{\partial f}{\partial k} dk = 0 \tag{13}$$

From (6)

$$dR_i = \frac{\partial R_i}{\partial \sigma_k} d\sigma_k + \frac{\partial R_i}{\partial \omega_j} d\omega_j \tag{14}$$

Substituting in (13)

$$\frac{\partial f}{\partial R_i}\left(\frac{\partial R_i}{\partial \sigma_k} d\sigma_k + \frac{\partial R_i}{\partial \omega_j} d\omega_j\right) + \frac{\partial f}{\partial k}\frac{\partial k}{\partial \bar{\omega}_p} d\bar{\omega}_p = 0 \tag{15}$$

Substituting (10) in (12)

$$d\bar{\omega}_p = C\left(d\lambda\left(\frac{\partial f}{\partial R_i}\frac{\partial f}{\partial R_i}\right)^{1/2}\right) \tag{16}$$

It can be shown that $\left(\frac{\partial f}{\partial R_i}\frac{\partial f}{\partial R_i}\right)^{1/2} = 1$ and for $C = 1$

$$d\bar{\omega}_p = d\lambda \tag{17}$$

Using (10), (11) and (17) in (15) and solving for $d\lambda$ yields

$$d\lambda = \frac{\frac{\partial f}{\partial R_i}\frac{\partial R_i}{\partial \sigma_k} d\sigma_k}{\frac{\partial k}{\partial \bar{\omega}_p} - \frac{\partial f}{\partial R_i}\frac{\partial R_i}{\partial \omega_j}\frac{\partial f}{\partial R_j}} \tag{18}$$

Introducing $H = \frac{\partial k}{\partial \bar{\omega}_p}$ = damage modulus, it can be measured experimentally in a uniaxial compression test and the same form is assumed for more general stress paths.

In the present work, H is expressed as a function of the distance between the loading and the bounding surface, given by

$$H = \frac{D\delta}{\langle \delta_{in} - \delta \rangle} \tag{19}$$

where $D = 2.65$ is a constant and < > are Macaulay brackets that set the quantity within it to zero if the value is negative. The normalized distance δ between the loading and bounding surfaces is given by

$$\delta = 1 - \frac{1}{b} \tag{20}$$

$\delta = \delta_{in}$ corresponds to R_o when the loading surface first crosses the limit fracture surface [24].

3 Incremental Stress-Strain Relations

3.1 Elasto-damage compliance matrix

Total form of stress-strain law can be expressed as

$$\varepsilon_i = \tilde{C}_{ij}(\omega_i)\,\sigma_j \tag{21}$$

The incremental form of Equation (21) is given by

$$d\varepsilon_i = \tilde{C}_{ij}\, d\sigma_j + \sigma_j \frac{\partial \tilde{C}_{ij}}{\partial \omega_k} d\omega_k \tag{22}$$

or

$$d\varepsilon_i = \tilde{C}_{ij}\, d\sigma_j + \sigma_j \frac{\partial \tilde{C}_{ij}}{\partial \omega_k} d\lambda \frac{\partial f}{\partial R_k} \tag{23}$$

$$d\varepsilon_i = \left\{\tilde{C}_{ij} + \sigma_l \frac{\partial \tilde{C}_{ij}}{\partial \omega_k}\frac{\partial f}{\partial R_k}\frac{d\lambda}{d\sigma_l}\right\} d\sigma_j \tag{24}$$

or

$$d\varepsilon_i = C_{ij}^{ed}\, d\sigma_j \tag{25}$$

where $d\lambda$ is defined in Equation (18), and C_{ij}^{ed} is the elasto-damage compliance matrix as defined in Equation (24). Equation (25) is useful in a stress control testing.

3.2 Elasto-damage stiffness matrix

The constitutive equation for strain control can be expressed as

$$\sigma_i = D_{ij}(\omega_i)\varepsilon_j \tag{26}$$

where

$$D = \tilde{C}^{-1} \tag{27}$$

Also we need

$$R_i = -\rho \frac{\partial W}{\partial \omega_i}(\varepsilon_i, \omega_i) \tag{28}$$

where,

$$\rho W = \frac{1}{2}[\varepsilon][D][\varepsilon]\ , \tag{29}$$

the complementary strain energy density.

$$dR_i = \frac{\partial R_i}{\partial \varepsilon_j} d\varepsilon_j + \frac{\partial R_i}{\partial \omega_j} d\omega_j \tag{30}$$

and

$$d\lambda = \frac{\dfrac{\partial f}{\partial R_k}\dfrac{\partial R_k}{\partial \varepsilon_j} d\varepsilon_j}{H - \dfrac{\partial f}{\partial R_k}\dfrac{\partial R_k}{\partial \omega_j}\dfrac{\partial f}{\partial R_j}} \tag{31}$$

The incremental form of Equation (26) is given by

$$d\sigma_i = D_{ij}\, d\varepsilon_j + \varepsilon_j \left\{ \frac{\partial D_{ij}}{\partial \omega_k} d\lambda \frac{\partial f}{\partial R_k} \right\} \tag{32}$$

$$d\sigma_i = \left\{ D_{ij} + \varepsilon_l \frac{\partial D_{ij}}{\partial \omega_k} \frac{\partial f}{\partial R_k} \frac{d\lambda}{d\varepsilon_l} \right\} d\varepsilon_j \tag{33}$$

or

$$d\sigma_i = D_{ij}^{ed}\, d\varepsilon_j \tag{34}$$

where $d\lambda$ is defined in Equation (31), and D_{ij}^{ed} is the elasto-damage stiffness matrix as defined explicitly in Equation (33). Equation (34) is useful in strain control testing.

4 Application of Proposed Elasto-Damage Model

4.1 Uniaxial compression

The strain energy density $\rho\Lambda$ for uniaxial compression is given by

$$\rho\Lambda = \frac{1}{2} \begin{bmatrix} \sigma & 0 & 0 \end{bmatrix} \left[\tilde{C}\right] \begin{bmatrix} \sigma \\ 0 \\ 0 \end{bmatrix} \tag{35}$$

Substituting for the compliance $\left[\tilde{C}\right]$, and setting $\alpha = 0$ (as it is used primarily as a parameter for matching peak strengths in tension testing), one obtains

$$\rho\Lambda = \frac{\sigma^2}{2E_o} \frac{(1-\beta\omega_1)^2}{(1-\beta\omega_2)^2 (1-\beta\omega_3)^2} \tag{36}$$

The thermodynamic relation

$$\varepsilon_i = \frac{\partial(\rho\Lambda)}{\partial \sigma_i} \tag{37}$$

yields

$$\sigma = \varepsilon_1 E_o \frac{(1-\beta\omega_2)^2 (1-\beta\omega_3)^2}{(1-\beta\omega_1)^2} \tag{38}$$

Substitution of (38) in (36) yields

$$\rho W = \frac{\varepsilon_1^2 E_o}{2} \frac{(1-\beta\omega_2)^2 (1-\beta\omega_3)^2}{(1-\beta\omega_1)^2} \tag{39}$$

Using the relationship

$$R_i = -\frac{\partial(W)}{\partial \omega_i} \tag{40}$$

one obtains

$$R_1 = -\frac{\beta\varepsilon_1^2 E_o (1-\beta\omega_2)^2 (1-\beta\omega_3)^2}{(1-\beta\omega_1)^3} = 0 \quad (\text{since } R_i \not< 0) \tag{41}$$

$$R_2 = \frac{\beta\varepsilon_1^2 E_o (1-\beta\omega_2)(1-\beta\omega_3)^2}{(1-\beta\omega_1)^2} \tag{42}$$

$$R_3 = \frac{\beta\varepsilon_1^2 E_o (1-\beta\omega_2)^2 (1-\beta\omega_3)}{(1-\beta\omega_1)^2} \tag{43}$$

From symmetry, $\omega_2 = \omega_3 = \omega$ and $\omega_1 = 0$ by virtue of Equation (41), yields

$$R_2 = R_3 = \beta\varepsilon_1^2 E_o (1-\beta\omega)^3 \tag{44}$$

and

$$(R_i R_i)^{1/2} = \sqrt{2}\beta\varepsilon_1^2 E_o (1-\beta\omega)^3 \tag{45}$$

and

$$\left[\frac{\partial f}{\partial R_i}\right] = \begin{bmatrix} 0 & \dfrac{1}{\sqrt{2}} & \dfrac{1}{\sqrt{2}} \end{bmatrix} \tag{46}$$

Differentiating R_j with respect to ω_i and ε_i and substituting along with (46) into (31) yields

$$d\lambda = \frac{2\sqrt{2}\beta\varepsilon_1 E_o (1-\beta\omega)^3\, d\varepsilon_1}{\left(H + 3\beta^2\varepsilon_1^2 E_o (1-\beta\omega)^2\right)} \quad ; \quad d\omega_i = d\lambda \left[\frac{\partial f}{\partial R_i}\right] \tag{47}$$

Finally, Equation (33) yields incremental stress-strain relationship for strain control testing as

$$d\sigma = \left(E_o (BW)^4 - \frac{8(\beta^2\varepsilon_1^2 E_o^2 (BW)^6}{\left(H + 3\beta^2\varepsilon_1^2 E_o (BW)^2\right)} \right) d\varepsilon_1 \tag{48}$$

where $BW = (1-\beta\omega)$.

Similarly, it can be shown that proceeding in a similar way incremental stress-strain relationship for stress control testing can be expressed as

$$d\varepsilon_1 = \left(\frac{1}{E_o\,(BW)^4} + \frac{8\beta^2\sigma^2\,/(BW)^{10} * E_o^2}{\left(H - \dfrac{5\beta^2\sigma^2}{E_o\,(BW)^6} \right)} \right) d\sigma \qquad (49)$$

4.2 Uniaxial tension

Following the same logic as in the case of uniaxial compression, it can be shown that for strain control testing

$$d\sigma = \left(E_o\,(AW)^2 \; - \frac{4(\alpha^2\varepsilon_1^2 E_o^2\,(AW)^2}{(H + \alpha^2\varepsilon_1^2 E_o)} \right) d\varepsilon_1 \qquad (50)$$

where $AW = (1-\alpha\omega_1)$, and for stress control testing

$$d\varepsilon_1 = \left(\frac{1}{E_o\,(AW)^2} + \frac{4\alpha^2\sigma^2\,/\,E_o^2\,(AW)^6}{\left(H - \dfrac{3\alpha^2\sigma^2}{E_o\,(AW)^4} \right)} \right) d\sigma \qquad (51)$$

4.3 Biaxial compression

Predictive ability of the proposed elasto-damage model for a multi-axial stress path is investigated for the biaxial stress state defined by $\sigma_1 = \sigma_2 = \sigma$. The 2×2 compliance and stiffness matrices for a general two-dimensional state of stress as a special case of Equations (1) are given by

$$\tilde{C}_{ij} = \tilde{C}_{ji} \qquad (i, j = 1,2) \text{ of Equation (1)}$$

whose inverse may be written as:

$$\tilde{D}_{11} = \frac{E_o(1-\alpha\omega_1)^2\,(1-\beta\omega_2)^2\,(1-\beta\omega_3)^2}{(1-\beta\omega_1)^2} \times \frac{(1-\gamma\omega_1)^2(1-\gamma\omega_2)^2}{\left\{(1-\gamma\omega_1)^2(1-\gamma\omega_2)^2 - \nu^2\right\}}$$

$$\tilde{D}_{22} = \frac{E_o(1-\alpha\omega_2)^2\,(1-\beta\omega_3)^2\,(1-\beta\omega_1)^2}{(1-\beta\omega_2)^2} \times \frac{(1-\gamma\omega_1)^2(1-\gamma\omega_2)^2}{\left\{(1-\gamma\omega_1)^2(1-\gamma\omega_2)^2 - \nu^2\right\}} \qquad (52)$$

$$\tilde{D}_{12} = \tilde{D}_{21} = E_o\,\nu\,(1-\alpha\omega_1)(1-\alpha\omega_2)(1-\beta\omega_3)^2 \times \frac{(1-\gamma\omega_1)(1-\gamma\omega_2)}{\left\{(1-\gamma\omega_1)^2(1-\gamma\omega_2)^2 - \nu^2\right\}}$$

Proceeding in a manner analogous to the uni-dimensional stress state, following is the resulting sequence of salient equations:

$$\rho\Lambda = \frac{\sigma^2}{E_o\,(1-\beta\omega_3)^2}\left(1 - \frac{\nu}{(1-\gamma\omega_1)(1-\gamma\omega_2)}\right) \qquad (53)$$

$$\varepsilon_1 = \frac{\sigma_1}{E_o}\,\frac{(1-\beta\omega_1)^2}{(1-\beta\omega_2)^2\,(1-\beta\omega_3)^2} - \frac{\nu\sigma_2}{E_o\,(1-\beta\omega_3)^2(1-\gamma\omega_1)(1-\gamma\omega_2)} \qquad (54)$$

Using $\sigma_1 = \sigma_2 = \sigma$, the inversion of Equation (54) yields

$$\sigma = \frac{\varepsilon_1 E_o\,(1-\beta\omega_3)^2}{\left(1 - \dfrac{\nu}{(1-\gamma\omega_1)(1-\gamma\omega_2)}\right)} \qquad (55)$$

Also

$$R_1 = R_2 = -\frac{2\nu\gamma\sigma^2}{E_o(1-\beta\omega_3)^2(1-\gamma\omega_1)^5} = 0 \qquad (56)$$

Components R_1 and $R_2 = 0$ due to the non-negativity of ω_i. Also

$$R_3 = \frac{2\beta\varepsilon_1^2 E_o(1-\beta\omega_3)}{(1-\nu)} \qquad (57)$$

Following the same steps as for uniaxial case, together with $\omega_1 = \omega_2 = 0$ and $\omega_3 = \omega$, leads to the following incremental σ–ε relationship for equal biaxial compression

$$d\sigma = \left(\frac{E_o(1-\beta\omega)^2}{(1-\nu)} - \frac{8\beta^2\varepsilon_1^2 E_o^2(1-\beta\omega)^2\,/(1-\nu)^2}{\left(H + \dfrac{2\beta^2\varepsilon_1^2 E_o}{(1-\nu)} \right)} \right) d\varepsilon \qquad (58)$$

This form is useful for strain control, however, for stress control the procedure will be similar to that for uniaxial case. The incremental stress-strain relationship for equal biaxial compression is expressed as

$$d\varepsilon = \left(\frac{(1-\nu)}{E_o(1-\beta\omega)^2} + \frac{8\beta^2\sigma^2(1-\nu)^2 / E_o^2(1-\beta\omega)^6}{\left(H - \frac{6\beta^2\sigma^2(1-\nu)}{E_o(1-\beta\omega)^4} \right)} \right) d\sigma \tag{59}$$

5 Determination of Regression Coefficients

The parameters α, β and γ are functions of initial modulus of elasticity, E_o, uniaxial compressive strength, f_c', and normalized strain invariants, $\frac{I_1}{\varepsilon_3}$ & $\frac{J_2}{e_3^2}$ (where $I_1 = \varepsilon_{kk}$ & $J_2 = \frac{1}{2} tr\,(e_{ij})$. Here, ε_3 and e_3 represent the minor principal and deviatoric strain, respectively. The suggested forms of α, β and γ are as follows:

$$\alpha = \alpha_0(f_c', E_o) + \alpha_1(f_c', E_o)\frac{I_1}{\varepsilon_3} + \alpha_2(f_c', E_o)\frac{J_2}{e_3^2} + \alpha_3(f_c', E_o)\frac{I_1}{\varepsilon_3}\frac{J_2}{e_3^2} \quad \text{(path dependent)} \quad (\sigma_1 > 0, \sigma_2 < 0) \tag{60}$$

or

$$\alpha = 0 \qquad (\sigma_1, \sigma_2 < 0)$$

$$\alpha = \overline{\alpha}(f_c', E_o) \qquad (\sigma_1, \sigma_2 \geq 0) \quad \text{(path independent)} \tag{61}$$

Phenomenological evidence is the essential guide in deciding if a particular stress state corresponds to a path dependent or path independent loading I_1, J_2 computed at the beginning of load increment.

$$\beta = \beta_0(f_c', E_o) + \beta_1(f_c', E_o)\frac{I_1}{\varepsilon_3} + \beta_2(f_c', E_o)\frac{J_2}{e_3^2} + \beta_3(f_c', E_o)\frac{I_1}{\varepsilon_3}\frac{J_2}{e_3^2} \quad \text{(path dependent)} \quad (\sigma_1, \sigma_2 < 0) \tag{62}$$

or

$$\beta = 0 \qquad (\sigma_1, \sigma_2 > 0)$$

$$\beta = \overline{\beta}(f_c', E_o) \qquad (\sigma_1 > 0, \sigma_2 < 0) \quad \text{(path independent)} \tag{63}$$

and

$$\gamma = \gamma(f_c', E_o) \qquad (\sigma_1, \sigma_2 < 0) \quad \text{(path independent)} \tag{64}$$

or

$$\gamma = 0 \qquad \text{(for all other stress states)}$$

where,

$$\alpha_i = \alpha_{i1} + \alpha_{i2} f_c' + \alpha_{i3} f_c'^2 + \alpha_{i4} E_o \quad , \quad (i = 0,1,2,3) \quad \text{path dependent} \tag{65}$$

$$\beta_i = \beta_{i1} + \beta_{i2} f_c' + \beta_{i3} f_c'^2 + \beta_{i4} E_o \quad , \quad (i = 0,1,2,3)$$

$$\alpha = \overline{\alpha}_0 + \overline{\alpha}_1 f_c' + \overline{\alpha}_2 f_c'^2 + \overline{\alpha}_3 E_o$$

$$\beta = \overline{\beta}_0 + \overline{\beta}_1 f_c' + \overline{\beta}_2 f_c'^2 + \overline{\beta}_3 E_o \quad \text{path independent} \tag{66}$$

$$\gamma = \gamma_0 + \gamma_1 f_c' + \gamma_2 f_c'^2 + \gamma_3 E_o$$

These parameters were calibrated by regressing against experimental σ–ε data for different f_c'. The range of f_c' used in regression varies from 4,000 psi to 17,400 psi, and is listed in Table 1. Stress paths used in regression are listed in Table 2.

f_c' (psi)	E_o (10^6 psi)	ν_o
4000	3.605	0.19
9434	6.023	0.19
13062	6.444	0.19
17416	7.126	0.19

ACI Equation $E_c = 57000\sqrt{f_c'}$ (f_c' in psi)

$= 4730\sqrt{f_c'}$ (f_c' in MPa)

Wee *et al.* [32] $E_c = 102000\,(f_c')^{1/3}$ (f_c' in MPa)

Table 1: Range of f_c' used in regression

σ_1/σ_2 for α	σ_1/σ_2 for β
–1	0
–0.25	0.2
–0.125	0.5
–0.1	0.8
–0.075	1.0
–0.05	
–0.025	

Table 2: Stress paths for determination of α, β

Regression was carried out in two steps as illustrated by Desai [30] and shown in Figure 1. In the first step, for a particular f_c' and E_o, α or β is determined by matching the peak stress to experimental data for varying stress ratios σ_1/σ_2. Then this data is regressed using the proposed form of α or β (Equations (60) & (62)) to obtain α_0, α_1, α_2, α_3 or β_0, β_1, β_2, β_3. At the end of this step, one has a set of α_i's and β_i's, where i = 0,1,2,3.

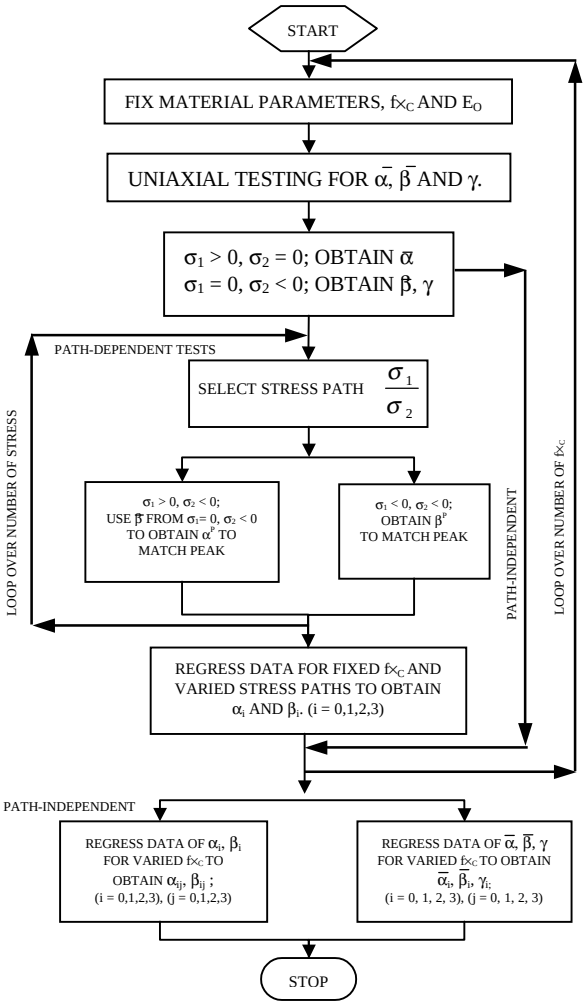

Figure 1: Flow chart for two-step regression

This process is then repeated for all the listed f_c'. The sets of α_i's and β_i's are then further regressed using the proposed functional forms of α_i's and β_i's (Equation (65)) to obtain α_{i1}, α_{i2}, α_{i3}, α_{i4} or β_{i1}, β_{i2}, β_{i3}, β_{i4}.

For determination of γ_i's and the path independent $\bar{\alpha}, \bar{\beta}$, regression is carried only once, since these parameters are presumed to be a function only of f_c' and E_o.

Final form of α_i's, β_i's and γ is as follows:

- α for path-dependent stress states

$$\begin{aligned}\alpha_0 &= -1.989\text{E}+01+1.788\text{E}-03*f_c'-5.644\text{E}\\ &\quad -08*f_c'^2+4.758\text{E}-07*E_o\end{aligned}$$

$$\begin{aligned}\alpha_1 &= -3.495\text{E}+01-1.445\text{E}-04*f_c'-4.415\text{E}\\ &\quad -09*f_c'^2+4.593\text{E}-06*E_o\end{aligned} \qquad (67)$$

$$\begin{aligned}\alpha_2 &= 2.825\text{E}+01-2.561\text{E}-03*f_c'+8.123\text{E}\\ &\quad -08*f_c'^2-6.864\text{E}-07*E_o\end{aligned}$$

$$\begin{aligned}\alpha_3 &= 4.47\text{E}+01+4.331\text{E}-04*f_c'-1.398\text{E}\\ &\quad -08*f_c'^2-6.109\text{E}-06*E_o\end{aligned}$$

- α for path-independent stress states

$$\begin{aligned}\alpha &= 1.116\text{E}+01-1.153\text{E}-03*f_c'+3.707\text{E}\\ &\quad -08*f_c'^2-1.514\text{E}-07*E_o\end{aligned} \qquad (68)$$

- β for path-dependent stress states

$$\begin{aligned}\beta_0 &= 3.6471\text{E}-01-2.6416\text{E}-05*f_c'+8.2457\text{E}\\ &\quad -10*f_c'^2-1.6974\text{E}-08*E_o\end{aligned}$$

$$\begin{aligned}\beta_1 &= -6.7164\text{E}-02+6.0082\text{E}-06*f_c'-1.7121\text{E}\\ &\quad -10*f_c'^2+8.3786\text{E}-10*E_o\end{aligned} \qquad (69)$$

$$\begin{aligned}\beta_2 &= -1.2177\text{E}-01-1.5589\text{E}-05*f_c'-4.1993\text{E}\\ &\quad -10*f_c'^2-5.7088\text{E}-09*E_o\end{aligned}$$

$$\begin{aligned}\beta_3 &= 6.1923\text{E}-02-8.7543\text{E}-06*f_c'+2.3097\text{E}\\ &\quad -10*f_c'^2+4.3012\text{E}-09*E_o\end{aligned}$$

- β for path-independent stress states

$$\begin{aligned}\beta &= 2.516\text{E}-01-1.978\text{E}-05*f_c'+6.421\text{E}\\ &\quad -10*f_c'^2-1.152\text{E}-08*E_o\end{aligned} \qquad (70)$$

- γ for path-independent stress states

$$\begin{aligned}\gamma &= 1.5863-1.221\text{E}-04*f_c'+3.4586\text{E}-09*f_c'^2\\ &\quad +5.3091\text{E}-08*E_o\end{aligned} \qquad (71)$$

Depending on the state of stress (σ_1, σ_2), the following combinations of α, β and γ are proposed as shown in Table 3.

6 Results

Results predicted by the proposed model discussed in earlier sections are verified for uniaxial and biaxial loading conditions by comparing them with the available experimental results. A strain control programme is used for plotting curves for predicted stress-strain response, volumetric dilatation and apparent Poisson's ratio for

State of stress	α	β	γ
$\sigma_1 > 0, \sigma_2 \geq 0$	$\bar{\alpha}(f_c', E_o)$	0	0
$\sigma_1 > 0, \sigma_2 < 0$	$\alpha\left(f_c', E_o, \frac{I_1}{\varepsilon_3}, \frac{J_2}{e_3^2}, \frac{I_1}{\varepsilon_3} * \frac{J_2}{e_3^2}\right)$	$\bar{\beta}(f_c', E_o)$	0
$\sigma_1 \leq 0, \sigma_2 \leq 0$	0	$\beta\left(f_c', E_o, \frac{I_1}{\varepsilon_3}, \frac{J_2}{e_3^2}, \frac{I_1}{\varepsilon_3} * \frac{J_2}{e_3^2}\right)$	$\gamma(f_c', E_o)$

Table 3: Combinations of α, β and γ

multiaxial loading conditions and is shown schematically in Figure 2.

Three different concretes (concrete A, f_c' = 4,000 psi (27.6 MPa), concrete B, f_c' = 9,434 psi (65 MPa) and concrete C, f_c' = 17,416 psi (120 MPa) were selected for comparison of predicted results of the model under uniaxial and biaxial loading conditions. For the case of uniaxial compression, comparison with experimental results of Wischers [31] and Wee *et al.* [32] shows that the predicted curves for concretes A and B (Figures 3 and 4) are stiffer and less ductile than the experimental curves i.e. the predicted peak stress compares quite well but the strains are somewhat on the lesser side. This can be attributed to the absence of plastic strains. Additional plastic strains will shift the curves to the right, making it comparable with the experimental values. Curve for concrete C, Figure 5, is in close agreement with the experimental curve [32] both in terms of peak stress and peak strain. It is evident from Figures 3–5 that the model can capture the increasing brittleness and decreasing ductility with the increase in uniaxial compressive strength quite effectively.

Figures 3–7 reflect the predictive capability of the model to capture the phenomenological behaviour of volumetric dilatation. In Figures 3–5, curves for lateral strains are shown in which the increase in lateral strains as the stress reaches the peak stress is clearly visible. This increase in lateral strains is due to the dramatic increase in apparent Poisson's ratio (Figure 6), which results in the change of sign of dilatancy (volumetric strain) as shown in Figure 7. It can be seen from the figure that under compression concrete always exhibits this phenomenon irrespective of the stress paths. Figure 6 represents the change in Poisson's ratio for all the three concretes. The curves are similar to the ones predicted by Krajcinovic and Fonseka [15] and Voyiadjis and Abu-Lebdeh [25]. Curves predicted in the present study are more consistent with the observed behaviour since the change in Poisson's ratio is more evident near the peak stress, while the change in Poisson's ratio is evident right from the onset of damage in the curves predicted by Krajcinovic and Fonseka [15] and Voyiadjis and Abu-Lebdeh [25].

For the case of uniaxial tension, softening in post-peak zone of stress-strain plots for all the concretes has been captured by the model effectively as shown in Figure 8. Shapes of the stress-strain plots correlate with the experimental results of Gopalaratnam and Shah [33].

For the case of biaxial compression, comparison with the experimental results of Kupfer *et al.* [34], Figures 9 and 10, indicates that the predicted peak stress envelope is in close agreement with the experimental peak stress.

It should be noted that this remarkable correlation with experimental data was obtained by introducing three parameters (α, β and γ) in the effective compliance matrix $\tilde{C}$, on the basis of available 2-D data for concrete. Since it is already shown that this rather simple approach is capable of capturing almost all the observed phenomenological trends of concrete, incorporation of more three dimensional data will yield a more rigorous model capable of predicting multiaxial behaviour of concrete.

7 Conclusions

An elasto-damage bounding surface model for monotonic behaviour of normal and high strength concrete is developed in this paper. A generalized compliance matrix is proposed in the principal coordinate system based on phenomenological evidences and physical insight. Typical behavioural trends of concrete are taken into account by

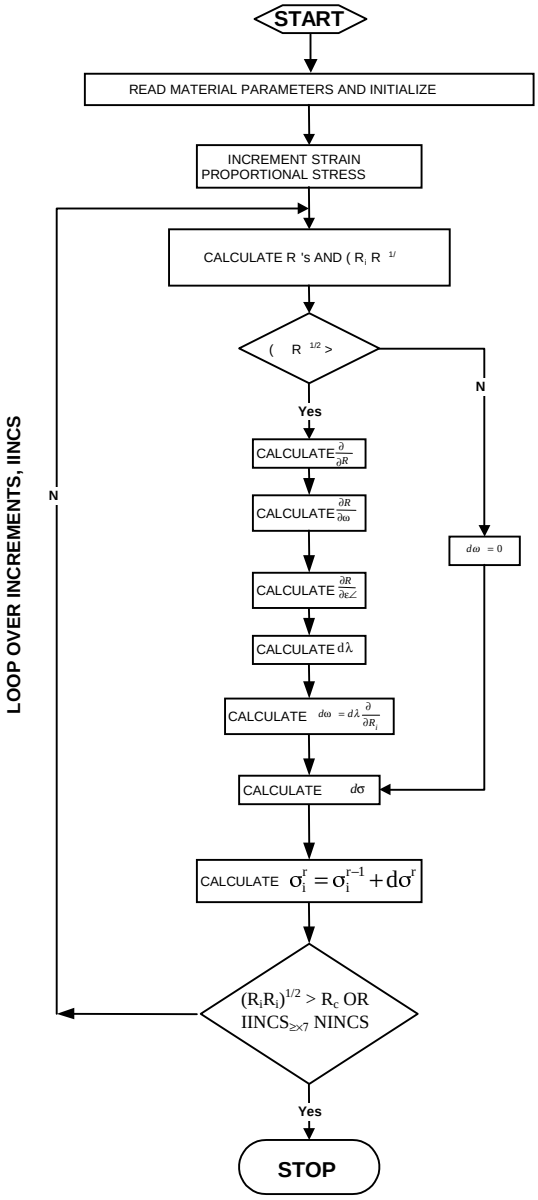

Figure 2: Flow chart for strain control programme

introducing three new parameters α, β and γ in the proposed compliance matrix.

Results presented in the paper demonstrate that the proposed model predicts the behaviour of concrete under multiaxial monotonic loadings adequately. Almost all the essential features of concrete including the volumetric dilatation are captured by the model. Absence of plastic strains has resulted in stiffer stress-strain curves, therefore, it is recommended to include the effect of plastic deformation in modelling the behaviour of concrete.

In order to make the model general and applicable to real three dimensional problems, work is in progress and more triaxial data will be incorporated in determining the regression coefficients.

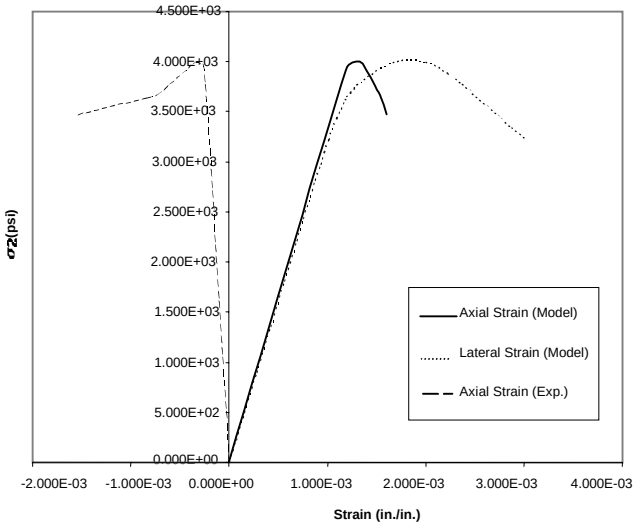

Figure 3: Stress-strain curves for uniaxial compression (f_c' = 4000 psi)

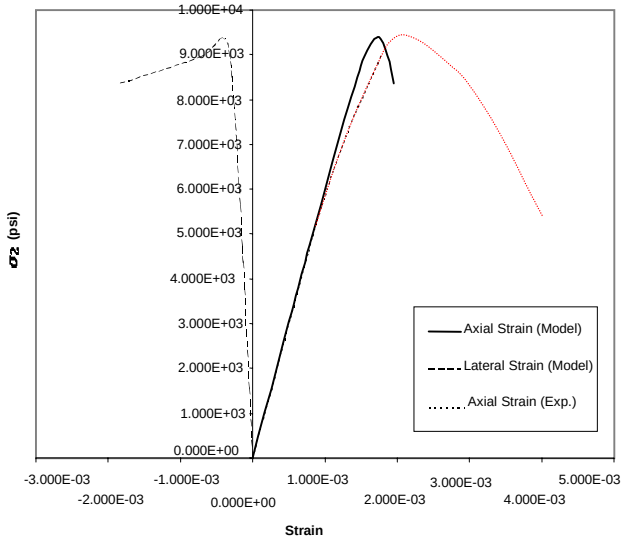

Figure 4: Stress-strain curves for uniaxial compression (f_c' = 9434 psi)

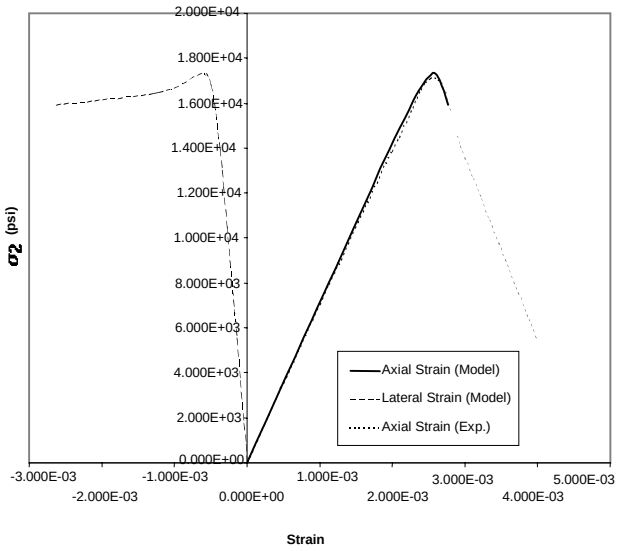

Figure 5: Stress-strain curves for uniaxial compression (f_c' = 17416 psi)

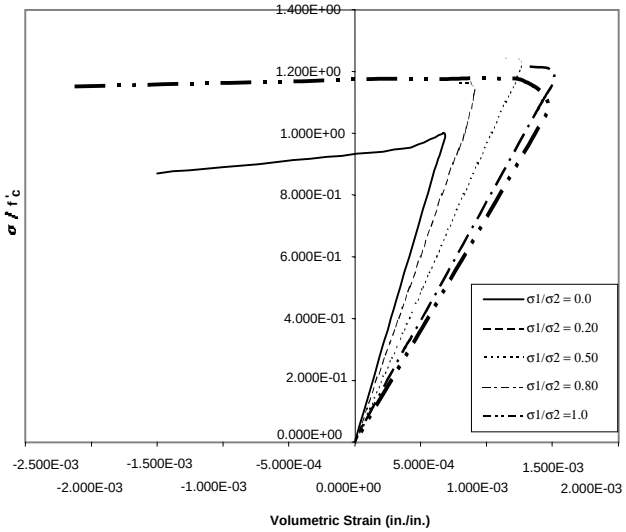

Figure 7: Volumetric dilatation for different stress paths (f_c' = 4000 psi)

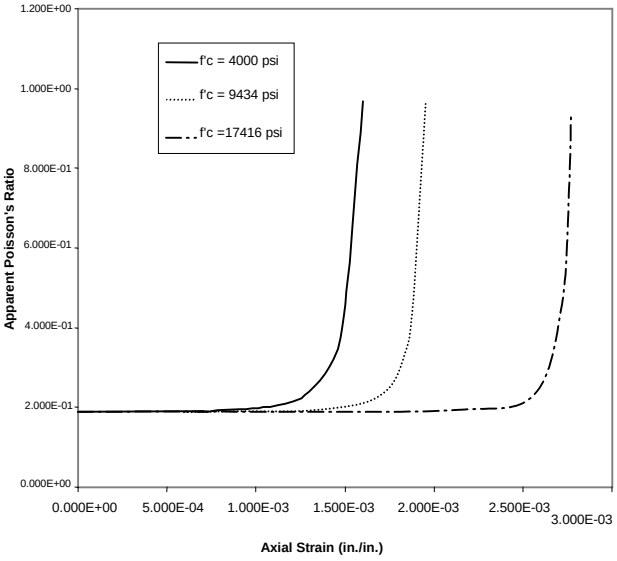

Figure 6: Apparent Poisson's ratio

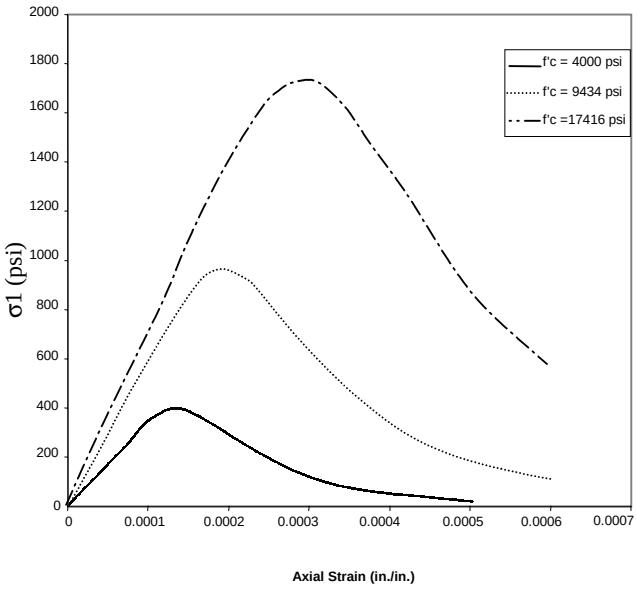

Figure 8: Stress-strain curves for uniaxial tension

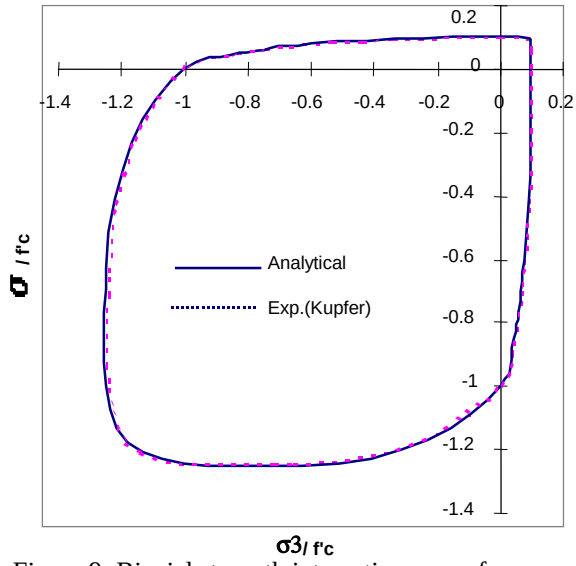

Figure 9: Biaxial strength interaction curve for concrete (f_c' = 4000 psi)

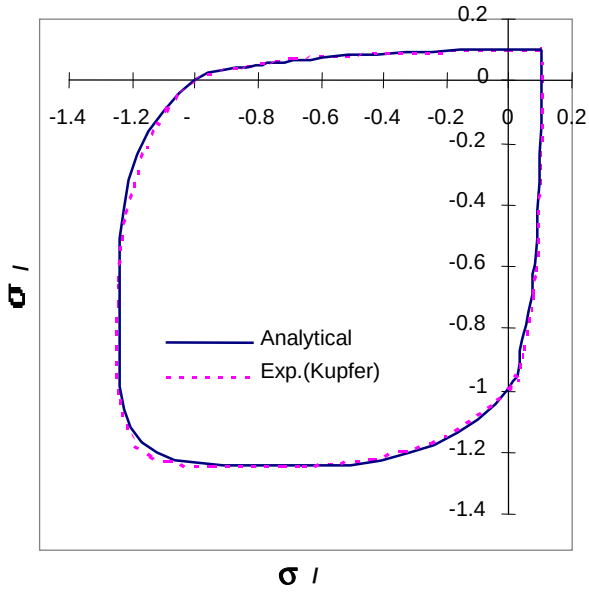

Figure 10: Biaxial strength interaction curve for concrete (f_c' = 9434 psi)

Acknowledgement

The authors are indebted to the Department of Civil Engineering, King Fahd University of Petroleum & Minerals, for their support in the pursuit of this work.

References

[1] Cedolin, L., Crutzen, Y.R.J., and Poli, S.D., "Triaxial stress-strain relationships for concrete", *J. Engg. Mech. Div. ASCE*, 103(EM3), 423-439, 1977.

[2] Liu, T.C.Y., Nilson, A.H., and Slate, F.O., "Biaxial stress-strain relations for concrete", *J. Struct. Div. ASCE*, 98(ST5), 1025-1034, 1972.

[3] Palaniswamy, R. and Shah, S.P., "Fracture and stress-strain relationship of concrete under triaxial compression", *J. Struct. Div. ASCE*, 100(ST5), 901-916, 1974.

[4] Chen, A.C.T. and Chen, W.F., "Constitutive relations for concrete", *J. Engg. Mech. Div. ASCE*, 101(EM4), 465-481, 1975.

[5] William, K.J. and Warnke, E.P., "Constitutive model for the triaxial behavior of concrete", *Proc. of IABSE Seminar on Concrete Structures Subjected to Triaxial Stress*, Bergamo, Italy, 1-31, 1975.

[6] Han, D.J. and Chen, W.F., "A nonuniform hardening plasticity model for concrete materials", *Mech. Materials*, 4, 283-302, 1985.

[7] Bazant, Z.P. and Bhat, P.D., "Endochronic theory of inelasticity and failure of concrete", *J. Engg. Mech. Div. ASCE*, 102(EM4), 701-722, 1976.

[8] Bazant, Z.P. and Shieh, C.L., "Endochronic model for nonlinear triaxial behaviour of concrete", *Nucl. Engg. Design*, 47, 305-315, 1978.

[9] Bazant, Z.P. and Kim, S.S., "Plastic-fracturing theory for concrete", *J. Engg. Mech. Div. ASCE*, 105(EM3), 407-428, 1979.

[10] Dragon, A. and Mroz, Z., "A continuum model for plastic-brittle behaviour of rock and concrete", *Int. J. Engg. Sci.*, 17, 121-137, 1979.

[11] Kachanov, L.M., "Time of the rupture process under creep conditions", *Izv Akad. Nauk*, U.S.S.R., Otd. Tekh. Nauk, 8, 26-31, 1958.

[12] Krajcinovic, D., "Constitutive equations for damaging materials", *J. Appl. Mech.*, ASME, 50, 355-360, 1983.

[13] Loland, K.E., "Continuous damage model for load-response estimation of concrete", *Cement and Conc. Res.*, 10(3), 26-31, 1980.

[14] Mazars, J., "Mechanical damage and fracture of concrete structure", *Advances in Fracture Mechanics (Fracture 81)*, Pergamon Press, Elmsford, N.Y., 1499-1506, 1981.

[15] Krajcinovic, D. and Fonseka, U., "The continuous damage theory for brittle materials, I and II", *J. Appl. Mech.*, 48(4), 809-824, 1981.

[16] Suaris, W. and Shah, S.P., "A rate sensitive damage theory for brittle solids", *J. Engg. Mech.*, ASCE, 110(6), 985-997, 1984.

[17] Kachanov, L.M., "Continuum model of medium with cracks", *J. Engg. Mech. Div. ASCE*, 106(EM5), 1039-1051, 1980.

[18] Cordebois, J.P. and Sidoroff, F., "Anisotropic damage in elasticity and plasticity", *J. Méc. Théor. Appl.*, Numéro Spécial, 45-60, 1982 (in French).

[19] Ortiz, M., "A constitutive theory for the inelastic behavior of concrete", *Mech. Materials*, 4(1), 67-93, 1985.

[20] Chow, C.L. and Wang, J., "An anisotropic theory of elasticity for continuum damage mechanics", *Int. J. Fracture*, 33, 3-16, 1987.

[21] Chow, C.L. and Wang, J., "An anisotropic theory of continuum damage mechanics for ductile fracture", *Engg. Fract. Mech.*, 27(5), 547-558, 1987.

[22] Dafalias, Y.F. and Popov, E.P., "Cyclic loading for material with a vanishing elastic region", *Nucl. Engg. Design*, 44, 293-302, 1977.

[23] Fardis, M.N., Alibe, B., and Tassoulas, J.L., "Monotonic and cyclic constitutive law for concrete", *J. Engg. Mech.*, ASCE, 109(2), 516-536, 1983.

[24] Suaris, W., Onyang, C., and Fernando, V.M., "Damage model for cyclic loading of concrete", *J. Engg. Mech.*, ASCE, 116(5), 1020-1035, 1990.

[25] Voyiadjis, G.Z. and Abu-Lebdeh, T.M., "Damage model for concrete using bounding surface concept", *J. Engg. Mech.*, ASCE, 119(9), 1865-1885, 1993.

[26] Abu-Lebdeh, T.M. and Voyiadjis, G.Z., "Plasticity-damage model for concrete under cyclic multiaxial loading", *J. Engg. Mech.*, ASCE, 119(7), 1465-1484, 1993.

[27] Yazdani, S. and Schreyer, H.L., "Combined plasticity and damage mechanics model for plain concrete", *J. Engg. Mech.*, ASCE, 116(7), 1435-1450, 1990.

[28] Yazdani, S. and Karnawat, S., "A constitutive theory for brittle solids with application to concrete", *Int. J. Damage Mech.*, 5(1), 93-110, 1996.

[29] Khan, A.R., Al-Gadhib, A.H., and Baluch, M.H., "An elasto-damage constitutive model for high-strength concrete", *Proc. of the Euro-C 1998 Conference on Computational Modelling of Concrete Structures*, Badgastein, Austria, 133-142, April 1998.

[30] Desai, C.S. and Siriwardane, H.J., *Constitutive Laws for Engineering Materials with Emphasis on Geologic Materials*, Prentice-Hall, Inc., Englewood Cliffs, N.J., 114-120, 1984.

[31] Wischers, G., "Application of effects of compressive loads on concrete", *Beton Technische Berichte*, No. 2 and 3, Duesseldorf, Germany, 1978.

[32] Wee, T.H., Chin, M.S., and Mansur, M.A., "Stress-strain relationship of high-strength concrete in compression", *J. Matls. Civil Engg.*, 8(2), 70-76, 1996.

[33] Gopalaratnam, V.S. and Shah, S.P., "Softening response of plain concrete in direct tension", *ACI Journal*, 82(3), 310-323, 1985.

[34] Kupfer, H., Hilsdorf, H.K., and Rusch, H., "Behavior of concrete under biaxial stresses", *ACI Journal, Proceedings*, 66(8), 656-666, 1969.